Int. J. Heat Mass Transfer. Vol. 36, No. 11, pp. 2869–2880, 1993
Printed in Great Britain

0017–9310/93 $6.00 + 0.00

Solidification of porous medium saturated with aqueous solution in a rectangular cell

K. MATSUMOTO,† M. OKADA,† M. MURAKAMI‡ and Y. YABUSHITA†

† Department of Mechanical Engineering, Aoyamagakuin University, 6-16-1 Chitosedai Setagaya-ku Tokyo 157, Japan

‡ Toshiba Corporation, 1-1-1 Shibaura Minato-ku Tokyo 105-01, Japan

(*Received* 20 *July* 1992 *and in final form* 8 *October* 1992)

Abstract—Beads saturated with NaCl-solution used as porous medium were packed in a rectangular cell. The porous medium was solidified by cooling one of the vertical walls of the cell. The above solidification process was studied analytically and experimentally. The temperature and concentration distributions were measured for three kinds of beads with almost the same mean diameters. From both experimental and analytical results, the analysis, where permeability within the the mushy region was expressed as the n-th power of the volume fraction of the liquid phase, was found to simulate approximately the solidification process. The characteristics of the solidification process were clarified herein.

1. INTRODUCTION

A FUNDAMENTAL understanding of a solidification process of a porous medium saturated with a solution is important for several engineering practices. In civil engineering, when the ground-freezing technique is used in order to support ground in a tunnel near sea, the soil which contains sea water is solidified. In a latent heat of fusion thermal energy storage system, a solution is used as a phase change material in order to get a desired phase change temperature, and a high thermal conductivity material is packed in the cell with the phase change material in order to enhance the heat transfer rate.

Several studies of solidification [1–5] or melting [6–9] with natural convection or forced convection in a porous medium saturated with pure water, and those of solidification of a binary solution [10–12], have already been reported, but there are no studies of a solidification process within a porous medium saturated with a binary solution. In order to clarify the above phase-change processes, it is important to solve the following problems. Namely, in solidification or melting in a porous medium saturated with pure water, how does a flow in the porous medium affect the solidification process or the melting process? In solidification in an experimental cell saturated with a binary solution, how does a mushy region containing both the liquid and solid phases grow? How does natural convection caused by a temperature gradient and a concentration gradient (so-called double-diffusive convection) affect the solidification process? In solidification within a porous medium saturated with a binary solution, how does the permeability of a mushy region formed in a porous medium affect the solidification process? Finally, how does the double-diffusive convection affect the solidification process?

In the present paper, beads packed in a rectangular experimental cell are treated as a porous medium, and the porous medium saturated with NaCl-solution is solidified from one of the vertical walls of the cell. Such a solidification problem is studied by means of a numerical analysis and the experiment, varying the material of beads.

As stated above, in the process of solidification of a solution within a porous medium, it is supposed that one of the most important factors governing the solidification phenomenon is the permeability of the mushy region. But the permeability is difficult to measure because the value of the permeability changes as the mushy region grows. Physical parameters governing this permeability are still barely known. In the present paper, the permeability is expressed as the n-th power function of the volume fraction of the liquid phase in the mushy region. The process of the solidification of porous medium saturated with aqueous solution is clarified, by measuring and calculating the distributions of temperature, concentration in the cell, the rate of solidification and the heat fluxes passing through the cold and hot walls of the cell.

2. ANALYSIS

2.1. *Analytical model*

The rectangular cell which has a height of h and a width of L is shown in Fig. 1. Both the horizontal walls of the cell are insulated and the temperature of the left vertical wall is T_c and that of the right vertical wall is T_h ($T_h > T_c$). In the present model, packed beads in the cell can be considered to be a porous medium, and the pores between beads are filled with the NaCl-solution. After predetermined initial conditions of the temperature and concentration of the solution in the porous medium are established, the porous medium is solidified from the left vertical wall of the cell. In the solidification process three regions,

NOMENCLATURE

a thermal diffusivity [$m^2 s^{-1}$]
c specific heat [$kJ kg^{-1} K^{-1}$]
$(c\rho)_e$ effective heat capacity [$kJ m^{-3} K^{-1}$]
$(c\rho)_L$ heat capacity of solution [$kJ m^{-3} K^{-1}$]
$(c\rho)^*$ $(c\rho)_e/(c\rho)_L$
C concentration [wt(%)]
C_c saturated concentration at the temperature of the cold wall [wt(%)]
C_v mass concentration where $C_v = (0.02379C^2 + 7.051C + 999.5)C/100$ [$kg m^{-3}$]
C_{vw} saturated mass concentration at T_w [$kg m^{-3}$]
C_w saturated concentration at T_w [wt(%)]
D mass diffusivity [$m^2 s^{-1}$]
D_b mean diameter of beads [mm]
Fo Fourier number, $(t/h^2)(\lambda_{eL}/(c\rho)_L)$
$\mathbf{g}$ gravitational acceleration [$m s^{-2}$]
h height of the cell [m]
Δh latent heat of fusion [$kJ kg^{-1}$]
k permeability [m^2]
k_0 permeability before solidification [m^2]
k^* k/k_0
L width of the cell [m]
Le Lewis number, $a/D = (\lambda_{eL}/(c\rho)_L)(1/D)$
n exponent of equation (21)
Ra_c Rayleigh number, $\mathbf{g}\beta_c(C_{vw} - C_{vi})h^3/\nu(\lambda_{eL}/(c\rho)_L)(k_0/h^2)$
Ra_T Rayleigh number, $\mathbf{g}\beta_T(T_{iL} - T_w)h^3/\nu(\lambda_{eL}/(c\rho)_L)(k_0/h^2)$
Ste Stefan number, $(c\rho)_L(T_{iL} - T_w)/\rho_s\Delta h$
t time [s]
T temperature [°C]
T_B temperature of brine at cold wall [°C]
T_c temperature of cold wall [°C]
T_h temperature of hot wall [°C]
T_{iL} solidification temperature corresponding to the initial concentration [°C]
T_w temperature of cold wall after T_c becomes constant [°C]
u apparent velocity in x-direction [$m s^{-1}$]
U $(c\rho)_L uh/\lambda_{eL}$
v apparent velocity in y-direction [$m s^{-1}$]
V $(c\rho)_L vh/\lambda_{eL}$
x, y Cartesian coordinates [m].
X x/h
Y y/h.

Greek symbols
α $C_{vi}/(C_{vw} - C_{vi})$
β_c volumetric expansion coefficient [$1/(kg m^{-3})$]
β_T volumetric expansion coefficient [K^{-1}]
θ $(T - T_{iL})/(T_{iL} - T_w)$
θ_c $(T_c - T_{iL})/(T_{iL} - T_w)$
θ_e $(T_e - T_{iL})/(T_{iL} - T_w)$
θ_h $(T_h - T_{iL})/(T_{iL} - T_w)$
θ_i $(T_i - T_{iL})/(T_{iL} - T_w)$
λ_e effective thermal conductivity [$W m^{-1} K^{-1}$]
λ_e^* λ_e/λ_{eL}
μ coefficient of viscosity [$kg m^{-1} s^{-1}$]
ν kinetic viscosity [$m^2 s^{-1}$]
ρ density [$kg m^{-3}$]
π $(C_v - C_{vi})/(C_{vw} - C_{vi})$
π_e $(C_{ve} - C_{vi})/(C_{vw} - C_{vi})$
ϕ stream function [$m^2 s^{-1}$]
Ψ $\phi \cdot (c\rho)_L/\lambda_{eL}$
Φ porosity, $(V_0 - V_1)/V_0$
χ volume fraction of liquid phase when the porous medium is in a mushy state, or volume fraction of liquid phase and eutectic solid when the porous medium is in a eutectic state, $(V_0 - V_1 - V_2)/V_0$
ω eutectic fraction, V_3/V_0
$(\chi - \omega)$ volume fraction of liquid phase, $(\chi - \omega) = V_4/V_0$ where V_0 control volume in porous medium, $V_0 = V_1 + V_2 + V_3 + V_4$. V_1 volume of beads in the control volume, V_2 volume of pure ice in the control volume, V_3 volume of eutectic solid in the control volume, V_4 volume of liquid phase in the control volume.

Subscripts
e eutectic point
i initial value
L liquid region
S solid region.

that is, solid region, mushy region and liquid region exist together in the cell, as shown in Fig. 1. The natural convection within both the mushy region and the liquid region, caused by temperature and concentration gradients, is also considered.

2.2. *Fundamental equations*

The assumptions for the analysis are as follows.

(1) The analytical model is two-dimensional in x, y coordinates.

(2) The flow in the porous medium is governed by Darcy's law.

(3) The temperature-dependency of the properties is considered only in the buoyancy term.

(4) The temperature of a liquid in a certain pore between beads is equal to the temperature of beads surrounding the liquid.

(5) Local phase equilibrium in the mushy region is valid.

(6) The relation between the solidification temperature and the concentration of NaCl-solution, is

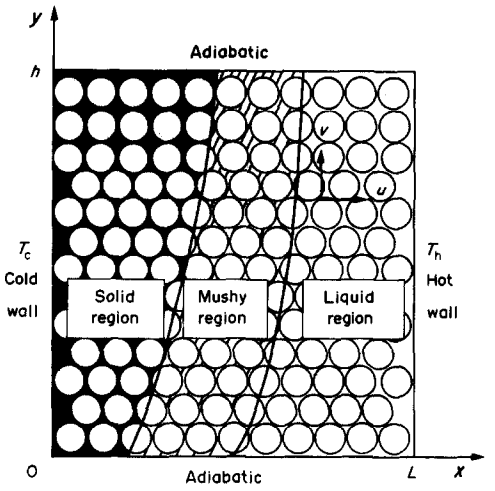

FIG. 1. Analytical model.

approximated by a straight line for the full range of this calculation.

(7) Mass diffusivity is constant.

(8) The viscous dissipation is neglected.

(9) The properties of a eutectic solid are equal to those of pure ice.

(10) Volume expansion due to phase change is negligible.

On the basis of the above assumptions, the governing equations, initial conditions, and boundary conditions are given as follows, where nondimensional parameters are described in the Nomenclature.

Effective values of thermal properties of porous medium.

$$\lambda_e = \frac{\chi-\omega}{\Phi}\lambda_{eL} + \left(1-\frac{\chi-\omega}{\Phi}\right)\lambda_{eS},$$

$$(c\rho)_e = \frac{\chi-\omega}{\Phi}(c\rho)_{eL} + \left(1-\frac{\chi-\omega}{\Phi}\right)(c\rho)_{eS}. \quad (1)$$

(Liquid region; $\chi = \Phi$, $\omega = 0$.)

Energy equation.

$$(c\rho)^*\frac{\partial\theta}{\partial Fo} + \frac{\partial U\theta}{\partial X} + \frac{\partial V\theta}{\partial Y} = \frac{\partial}{\partial X}\left(\lambda_e^*\frac{\partial\theta}{\partial X}\right) + \frac{\partial}{\partial Y}\left(\lambda_e^*\frac{\partial\theta}{\partial Y}\right). \quad (2)$$

Mass diffusion equation.

$$\chi\frac{\partial\pi}{\partial Fo} + \frac{\partial U\pi}{\partial X} + \frac{\partial V\pi}{\partial Y} = \frac{1}{Le}\left[\frac{\partial}{\partial X}\left(\chi\frac{\partial\pi}{\partial X}\right) + \frac{\partial}{\partial Y}\left(\chi\frac{\partial\pi}{\partial Y}\right)\right]. \quad (3)$$

Momentum equation.

$$\frac{\partial}{\partial X}\left(\frac{1}{k^*}\frac{\partial\Psi}{\partial X}\right) + \frac{\partial}{\partial Y}\left(\frac{1}{k^*}\frac{\partial\Psi}{\partial Y}\right) = -Ra_T\frac{\partial\theta}{\partial X} - Ra_c\frac{\partial\pi}{\partial X}. \quad (4)$$

Velocities.

$$U = \frac{\partial\Psi}{\partial Y}. \quad (5)$$

$$V = -\frac{\partial\Psi}{\partial X}. \quad (6)$$

(Mushy region; $\pi = -\theta$, $0 < \chi < \Phi$, $\omega = 0$.)

Energy equation.

$$(c\rho)^*\frac{\partial\theta}{\partial Fo} + \frac{\partial U\theta}{\partial X} + \frac{\partial V\theta}{\partial Y} = \frac{\partial}{\partial X}\left(\lambda_e^*\frac{\partial\theta}{\partial X}\right) + \frac{\partial}{\partial Y}\left(\lambda_e^*\frac{\partial\theta}{\partial Y}\right) - \frac{1}{Ste}\frac{\partial\chi}{\partial Fo}. \quad (7)$$

Mass diffusion equation.

$$\chi\frac{\partial\pi}{\partial Fo} + \frac{\partial U\pi}{\partial X} + \frac{\partial V\pi}{\partial Y} = \frac{1}{Le}\left[\frac{\partial}{\partial X}\left(\chi\frac{\partial\pi}{\partial X}\right) + \frac{\partial}{\partial Y}\left(\chi\frac{\partial\pi}{\partial Y}\right)\right] - (\pi+\alpha)\frac{\partial\chi}{\partial Fo}. \quad (8)$$

Momentum equation.

$$\frac{\partial}{\partial X}\left(\frac{1}{k^*}\frac{\partial\Psi}{\partial X}\right) + \frac{\partial}{\partial Y}\left(\frac{1}{k^*}\frac{\partial\Psi}{\partial Y}\right) = -Ra_T\frac{\partial\theta}{\partial X} - Ra_c\frac{\partial\pi}{\partial X}. \quad (9)$$

Velocities.

$$U = \frac{\partial\Psi}{\partial Y}. \quad (10)$$

$$V = -\frac{\partial\Psi}{\partial X}. \quad (11)$$

(Eutectic; $\theta = \theta_e$, $\pi = \pi_e$.)

Energy equation.

$$\frac{\partial U\theta}{\partial X} + \frac{\partial V\theta}{\partial Y} = \frac{\partial}{\partial X}\left(\lambda_e^*\frac{\partial\theta}{\partial X}\right) + \frac{\partial}{\partial Y}\left(\lambda_e^*\frac{\partial\theta}{\partial Y}\right) - \frac{1}{Ste}\frac{\partial(\chi-\omega)}{\partial Fo}. \quad (12)$$

Mass diffusion equation.

$$\frac{\partial U\pi}{\partial X} + \frac{\partial V\pi}{\partial Y} = \frac{1}{Le}\left[\frac{\partial}{\partial X}\left((\chi-\omega)\frac{\partial\pi}{\partial X}\right) + \frac{\partial}{\partial Y}\left((\chi-\omega)\frac{\partial\pi}{\partial Y}\right)\right] - (\pi+\alpha)\frac{\partial\chi}{\partial Fo}. \quad (13)$$

(Solid region.)

Energy equation.

$$(c\rho)^*\frac{\partial\theta}{\partial Fo} = \frac{\partial}{\partial X}\left(\lambda_e^*\frac{\partial\theta}{\partial X}\right) + \frac{\partial}{\partial Y}\left(\lambda_e^*\frac{\partial\theta}{\partial Y}\right). \quad (14)$$

I.C.

$$\theta = \theta_i, \quad \pi = 0, \quad U = V = \Psi = 0. \quad (15)$$

B.C.

$$\theta = \theta_c, \quad \pi = 0 \ (X = 0),$$

$$\Psi = 0 \text{ (on solid–mush interface)}. \tag{16}$$

$$\theta = \theta_h, \quad \frac{\partial \pi}{\partial X} = 0, \quad U = \Psi = 0 \quad (X = L/h). \tag{17}$$

$$\frac{\partial \theta}{\partial Y} = 0, \quad \frac{\partial \pi}{\partial Y} = 0, \quad V = \Psi = 0 \quad (Y = 0, Y = 1). \tag{18}$$

2.3. *Estimation of permeability within mushy region*

For the solidification of the solution within the porous medium, it is supposed that the main factor governing the phenomenon is permeability within the mushy region. But at present, the value of the permeability during the solidification of the solution is unknown.

In this paper, the value of permeability is estimated on the basis of Rumpf and Gupte's report [13]. In Rumpf and Gupte's report, permeability k within the porous medium is expressed by the following equation,

$$k = D_b^2 \Phi^{5.5}/(5.6K) \tag{19}$$

where Φ is porosity and is equal to the volume fraction of liquid phase before solidification. D_b is the mean diameter of beads, and K is constant. The volume fraction of liquid phase within the mushy region varies during the solidification of solution. Since ice formed between the beads with a growth of the mushy region is dendritic, the size of crystal of ice formed between beads is smaller than the mean diameter of the beads. Namely, as the crystal of the formed ice is considered to be smaller beads than the beads constituting the porous medium, the mean diameter of the beads and the ice becomes gradually smaller as the mushy region grows, therefore, it is supposed that in the process of solidification the exponent of equation (19) is larger than 5.5. From the above mentioned reason, the relationship between permeability and volume fraction of the liquid phase in the mushy region is assumed as follows:

$$k \propto \chi^n (n > 5.5) \tag{20}$$

where χ is the volume fraction of the liquid phase in the mushy region and if the solidification of solution does not occur, χ corresponds to Φ in equation (19). As, at least, the permeability in the process of solidification, depends on the volume fraction of the liquid phase in the mushy region, it is not so inaccurate physically and mathematically that the permeability is expressed as equation (20). Besides, in the measurement of the permeability [14], it was shown that $\log(k)$ was proportional to $\log(\chi)$. Equation (20) is normalized by using permeability before solidification, k_0, and the volume fraction of the liquid phase before solidification, Φ, as follows:

$$(k/k_0) = (\chi/\Phi)^n \tag{21}$$

where Φ corresponds to the so-called porosity within the porous medium before solidification.

Naturally, when (χ/Φ) is equal to 0, (k/k_0) is equal to 0, and when (χ/Φ) is equal to 1, (k/k_0) is equal to 1. Therefore, the relationship between (k/k_0) and (χ/Φ) can be shown as Fig. 2. In this paper, the exponent n of equation (21) governing the behavior of permeability in the process of solidification, is determined, as follows. The values of the permeability in the process of solidification is predicted conversely from the measured concentration of liquid region at the final phase of the experiment. Namely, in this paper the exponent n of $(\chi/\Phi)^n$ was determined by comparing the analytical results of concentration with the experimental ones in the period in which the rate of the concentration rise became almost stable after the initial period of solidification.

The comparison of analytical results of concentration with experimental results in the case of vinyl chloride beads with 3.76 mm mean diameter and $C_i = 10$ wt(%) is shown in Fig. 3(a). Details of the analysis and the experiment will be described in the following sections. The exponent n was determined on the basis of experimental results of concentration corresponding to symbol $\times$ in the period from $t = 300$ to 360 min when the rate of the concentration rise became stable, that was determined to be 14. From Fig. 3(a), the present analysis simulates approximately not only the latter half process of solidification but also the first half process of solidification. Similar comparisons under the same experimental conditions as Fig. 3(a), are shown in Figs. 3(b) and (c). In the case of Fig. 3(b), the exponent n was determined to be 1, corresponding to the simplest case shown in Fig. 2. As clarified from Fig. 3(b), a great difference between the analytical and experimental results arises, so it is not effective that the exponent n is determined

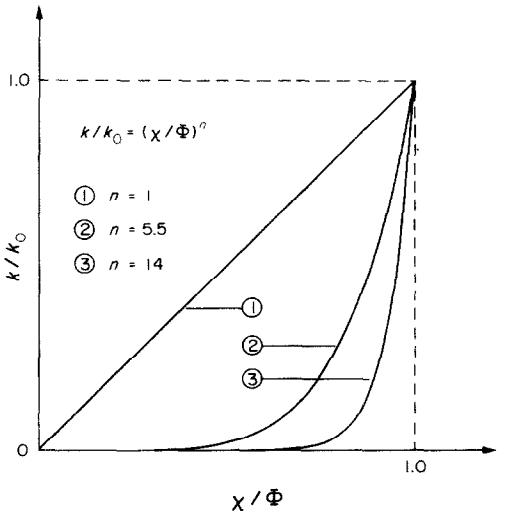

FIG. 2. Relationship between permeability and volume-fraction of liquid phase within mushy region.

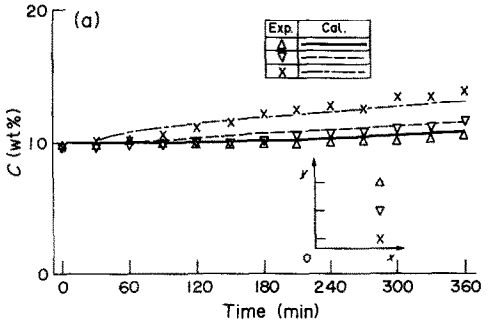

FIG. 3(a). Comparison of analytical results with experimental results in the case of vinyl chloride beads. (x, y); × (90 mm, 10 mm), ▽ (90, 50), △ (90, 90). $C_i = 10$ wt(%), $T_i = 0°C$, $T_B = -30°C$, $Ra_c = -4000$, $Ra_T = 29.4$, $D_b = 3.76$ mm, $\Phi = 0.362$, $k_0 = 7.04 \times 10^{-9}$ m^2, $n = 14$.

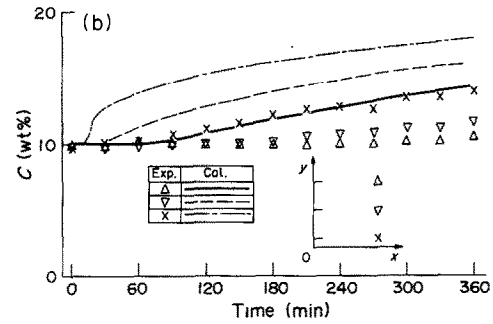

FIG. 3(b). Comparison of analytical results with experimental results in the case of vinyl chloride beads. (x, y); × (90 mm, 10 mm), ▽ (90, 50), △ (90, 90). $C_i = 10$ wt(%), $T_i = 0°C$, $T_B = -30°C$, $Ra_c = -4000$, $Ra_T = 29.4$, $D_b = 3.76$ mm, $\Phi = 0.362$, $k_0 = 7.04 \times 10^{-9}$ m^2, $n = 1$.

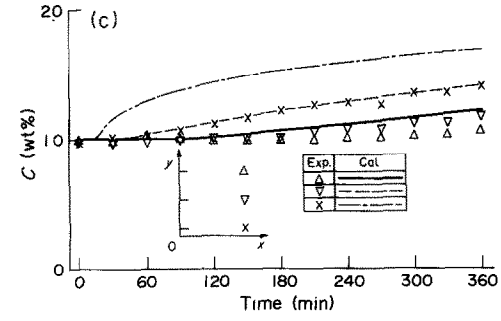

FIG. 3(c). Comparison of analytical results with experimental results in the case of vinyl chloride beads. (x, y); × (90 mm, 10 mm), ▽ (90, 50), △ (90, 90). $C_i = 10$ wt(%), $T_i = 0°C$, $T_B = -30°C$, $Ra_c = -4000$, $Ra_T = 29.4$, $D_b = 3.76$ mm, $\Phi = 0.362$, $k_0 = 7.04 \times 10^{-9}$ m^2, $n = 5.5$.

to be 1. In the case of Fig. 3(c), the component n was determined to be 5.5 on the basis of equation (20). As well as Fig. 3(b), a large difference between the analytical and experimental results appeared.

It was reported [14] that (k/k_0) was proportional to $(\chi/\Phi)^{12}$ when the permeability in a state of solidification of porous medium saturated with the solution for the case of vinyl chloride beads with 3.76 mm mean diameter and $C_i = 10$ wt(%) was measured under the condition that χ and the concentration were kept uniform, though in this model, the distributions of χ and concentration are not uniform due to the flow caused by temperature and concentration gradients, the difference between the value of the exponent n shown in this paper ($n = 14$) and that reported in ref. [14] ($n = 12$) is small.

As is evident from the above discussion, it is considered to be effective that (k/k_0) is expressed by $(\chi/\Phi)^n$ as shown in Fig. 2 and the exponent n of $(\chi/\Phi)^n$ is determined by comparing the analytical results of concentration with the experimental ones in the period in which the rate of the concentration rise becomes stable after the initial period of the solidification.

Naturally, the manner of ice growth formed in the mushy region is different, and the value of the permeability changes with the difference of the thermal conductivity of the beads. But in cases of steel and glass beads with almost the same mean diameters as vinyl chloride beads under the same experimental conditions as Fig. 3(a), the values of the exponent n were nearly equal to 14, as well as in the case of vinyl chloride beads. Namely, it is considered that the influence of the thermal conductivity of beads on (k/k_0) is very small in the present experimental cell which is small in size, such as the height and width of 100 mm and 100 mm, respectively.

In the following discussion, the exponent n was determined on the basis of the experimental results of concentration in the case of vinyl chloride beads with 3.56 mm diameter and $C_i = 10$ wt(%), and the numerical analysis was performed using $n = 14$.

2.4. *Calculation*

From the above equations, the temperature, concentration, volume fraction, stream function and freezing front are numerically calculated under the initial and boundary conditions by means of the explicit finite difference method (FDM), varying the material of the beads. For the calculation of the temperature distribution with a phase change, the enthalpy method is used. Stream function is calculated by using the SOR method, and the upwind finite difference scheme of first-order precision for velocity is adopted. In the analysis, the calculations are performed under the conditions that the number of divisions are 20 by 20 and 40 by 40; the number of divisions are determined to be 20 by 20 because the difference between both results of the calculations were small, considering the experimental precision. Therefore, the mesh sizes are equal to 0.05 in the nondimensional coordinates X, Y.

3. EXPERIMENT

3.1. *Experimental apparatus*

Three kinds of beads, made of glass, vinyl chloride and steel are chosen because of their thermal conductivities, namely, the thermal conductivity of steel is larger than that of ice, the thermal conductivity of

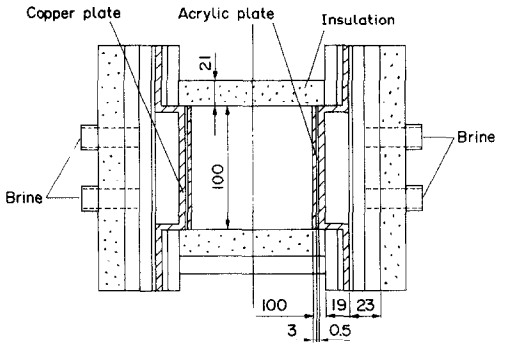

FIG. 4. Experimental cell.

glass is larger than that of water and lower than that of ice, and the thermal conductivity of vinyl chloride is lower than that of water.

The experimental cell is shown in Fig. 4. The cell is rectangular with the sectional area, 100 mm by 100 mm, and consists of the two horizontal walls made of acrylic plate, both right and left vertical walls made of copper plate, and the other two vertical walls made of acrylic plate, to observe the process of the solidification in the cell. The temperatures of the copper walls are controlled by letting brine at a constant temperature flow behind the copper walls. Both copper walls, between which acrylic plates 0.5 mm thick are sandwiched, are used as heat flux meters to measure the heat flux passing through the walls. In addition to this, the whole of the cell is covered with an insulation of styrene foam, 21 mm thick. The temperature is measured by C–C thermocouples of 0.2 mm diameter inserted into stainless steel tubes of 0.8 mm outer diameter. Fifty-five temperature measurement points were arranged in a staggered configuration. The temperatures of copper plates on both sides of the acrylic plates are also measured to obtain the heat flux. For measuring the local concentration of the solution in the liquid region, a mesh pipe made of the net is set vertically into the porous medium and about 0.25 ml of solution is sucked up by a syringe, and the concentration of the solution in the liquid region is measured by a concentration meter. The solution at a desired position of the mushy region cannot be sucked up by the syringe due to ice formed at the upper part of the mushy region, therefore the measurement of the concentration in the mushy region could not be performed. Namely, when the front of the mushy region reaches the measuring point of the concentration set at the upper part of the cell, the measurement of concentration is ended. The concentration in the liquid region is measured from two positions in the horizontal plane and three positions in the vertical plane.

3.2. *Experimental procedure*

Beads packed in the experimental cell are treated as a porous medium. The beads in the experimental cell are initially saturated with a solution of a predetermined concentration. The initial temperature of all experiments is 0°C. When the initial temperature distribution in the cell reaches within ± 0.5°C, the lower temperature brine is allowed to flow and the experiment is started. The temperature is measured every 2 min for the first 80 min after starting the experiment, and every 5 min for the next 80 min, and then every 10 min thereafter. The concentration is measured every 30 min throughout the experiment.

The above experimental procedure is repeated, varying the material of the beads. The properties of the beads used in this paper are shown in Table 1.

Table 1. Properties of beads

	Glass	Steel	Vinyl chloride
D_b (mm)	2.56	2.76	3.76
Φ	0.380	0.387	0.362
λ_{es} (W m^{-1} K^{-1})	1.47	6.99	0.72
λ_{el} (W m^{-1} K^{-1})	0.87	2.67	0.32
$C_i = 10$ wt(%)	$T_B = -30$°C	$T_i = T_h = 0$°C	

4. COMPARISON OF ANALYTICAL RESULTS WITH EXPERIMENTAL RESULTS AND DISCUSSION

In the following discussion, the experiment and the analysis were performed under the conditions of $C_i = 10$ wt(%), $T_i = T_h = 0$°C and $T_B = -30$°C.

Time-dependency of the temperature in the x direction at $y = 50$ mm is shown in Fig. 5, in the case of the vinyl chloride beads. In Fig. 5, the symbols show the experimental results, and the lines show the analytical results. In the analysis, the experimental results of temperature on the cold and hot walls are used as

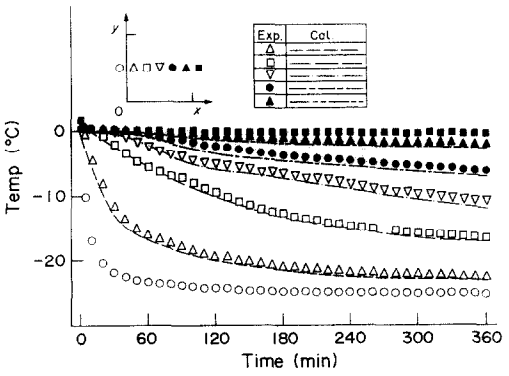

FIG. 5. Relationship between temperature at $y = 50$ mm and time in the case of vinyl chloride beads. (x, y); ○ (0 mm, 50 mm), △ (10, 50), □ (30, 50), ▽ (50, 50), ● (70, 50) ▲ (90, 50), ■ (100, 50). $C_i = 10$ wt(%), $T_i = 0$°C, $T_B = -30$°C, $Ra_c = -4000$, $Ra_T = 29.4$, $D_b = 3.76$ mm, $\Phi = 0.362$, $k_0 = 7.04 \times 10^{-9}$ m^2.

the boundary conditions. As is evident from Fig. 5, a good agreement between the experimental results and the analytical results was obtained. The relationship between temperature and time at $x = 50$ and 80 mm for the same experiment as Fig. 5 is shown in Fig. 6. As clarified from Fig. 6, a temperature difference between the upper part and the lower part of the cell caused by natural convection appears. The experimental and analytical results using various beads showed that this temperature difference increased with the decrease of effective thermal conductivity.

Time-dependencies of the concentration in the y direction are given in Figs. 7, 8 and 9, for steel beads, glass beads and vinyl chloride beads, respectively. The symbols, for example ◇, show the experimental results. The lines, for example the solid line, show analytical results. As stated in Section 3.1, when the front of the mushy region reached the measurement points, the measurement of the concentration was ended. In the case of Fig. 7, a good agreement between the analytical and experimental results was obtained. But in the cases of Figs. 8 and 9, at the lower part of the cell where the value of the concentration becomes the highest among the measuring points, small differences between the analytical results corresponding to the chain lines in case (2) of Figs. 8 and 9 and the experimental results corresponding to symbols × in case (2) of Figs. 8 and 9 arise. These differences suggested that there are some factors other than (χ/Φ) governing (k/k_0). From Figs. 5–9, though there are small differences between the analytical and experimental results, especially for concentration, the present analysis simulates approximately the process of solidification of a porous medium saturated with a solution in spite of the large difference of thermal conductivity of various beads. The solid line for case (1) in Fig. 7 rises rapidly at $t = 50$ min because the front of the mushy region reaches the measuring point of concentration at $t = 50$ min. Although for the solid lines shown in case (1) of Figs. 8 and 9 the rate of variation is smaller than that in case (1) of Fig. 7, because the growing rate of the freezing front in the

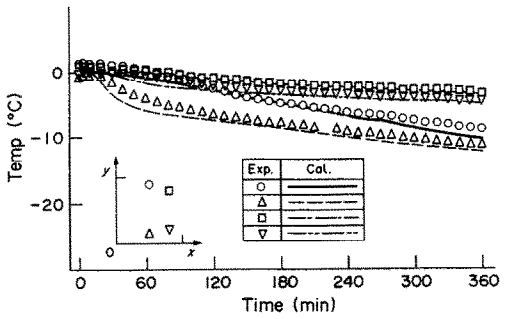

FIG. 6. Relationship between temperature at $x = 50$, 80 mm and time in the case of vinyl chloride beads. (x, y); △ (50 mm, 10 mm), ○ (50, 90), ▽ (80, 20), □ (80, 80). $C_i = 10$ wt(%), $T_i = 0°C$, $T_B = -30°C$, $Ra_c = -4000$, $Ra_T = 29.4$, $D_b = 3.76$ mm, $\Phi = 0.362$, $k_0 = 7.04 \times 10^{-9}$ m^2.

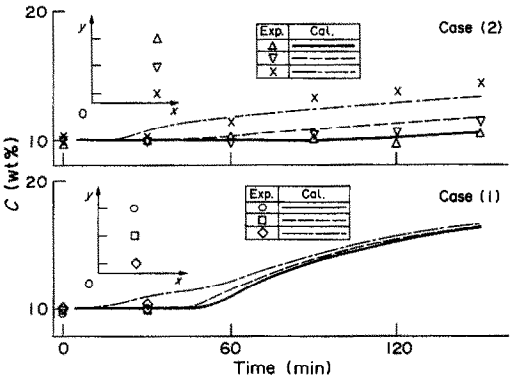

FIG. 7. Relationship between concentration and time in the case of steel beads. (x, y); ◇ (50 mm, 10 mm), □ (50, 50), ○ (50, 90), × (90, 10), ▽ (90, 50), △ (90, 90). $C_i = 10$ wt(%), $T_i = 0°C$, $T_B = -30°C$, $Ra_c = -53.4$, $Ra_T = 3.92$. $D_b = 2.76$ mm, $\Phi = 0.387$, $k_0 = 7.84 \times 10^{-9}$ m^2.

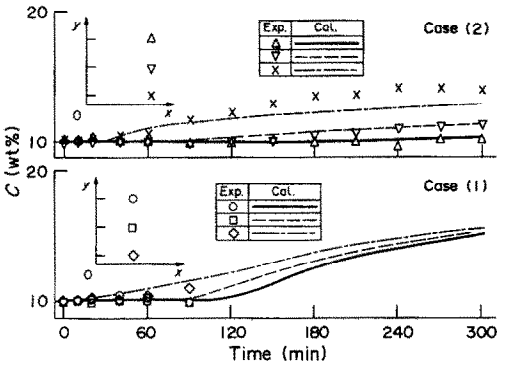

FIG. 8. Relationship between concentration and time in the case of glass beads. (x, y); ◇ (50 mm, 10 mm), □ (50, 50), ○ (50, 90), × (90, 10), ▽ (90, 50), △ (90, 90). $C_i = 10$ wt(%), $T_i = 0°C$, $T_B = -30°C$, $Ra_c = -1030$, $Ra_T = 7.58$, $D_b = 2.56$ mm, $\Phi = 0.38$, $k_0 = 5.00 \times 10^{-9}$ m^2.

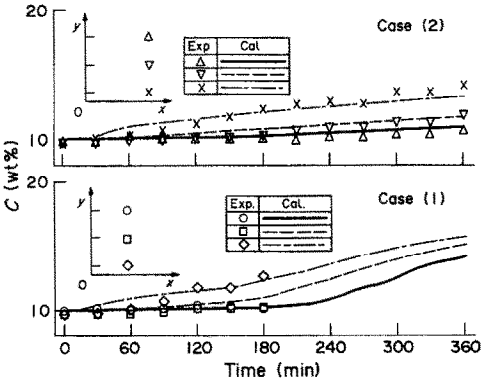

FIG. 9. Relationship between concentration and time in the case of vinyl chloride beads. (x, y); ◇ (50 mm, 10 mm), □ (50, 50), ○ (50, 90), × (90, 10), ▽ (90, 50), △ (90, 90). $C_i = 10$ wt(%), $T_i = 0°C$, $T_B = -30°C$, $Ra_c = -4000$, $Ra_T = 29.4$, $D_b = 3.76$ mm, $\Phi = 0.362$, $k_0 = 7.04 \times 10^{-9}$ m^2.

cases of glass and vinyl chloride beads is later than that in the case of steel beads, that is, in these cases the amount of solute per time rejected from the solution is larger, the characteristics of time-dependency of concentration are nearly the same for three kinds of beads with different properties, as shown by Figs. 7–9. The solute is rejected from the solution in the mushy region as the mushy region grows. A high concentration of the solution flows down through the mushy region and stays at the bottom of the cell. Consequently, a concentration stratification is formed in the liquid region. As clarified from the comparison of symbol ◇ corresponding to the experimental result at $t = 180$ min in case (1) of Fig. 9 with symbol × corresponding to the experimental one at $t = 180$ min in case (2) of Fig. 9, a concentration difference in the x-direction hardly appears, and from the comparison of symbol △ corresponding to the experimental result at $t = 360$ min of case (2) of Fig. 9 with symbol × corresponding to the experimental one at $t = 360$ min in case (2) of Fig. 9, it is found that the concentration stratification is formed in the y-direction. In the cases of Figs. 7 and 8, similar results are obtained.

For the case of vinyl chloride beads, the time-dependency of the isothermal line is given in Fig. 10. The isothermal lines are calculated by means of the interpolation of the experimental results and the analytical results. In Fig. 10(a), the calculated results of the temperature (shown by dashed lines) are smaller than the experimental ones (shown by solid lines) at the lower part of the liquid region and during the early period of solidification. It corresponds to the results that in Fig. 9 the analytical results of concentration at the lower part of the liquid region (corresponding to the chain lines) were larger than the experimental results (corresponding to symbols ◇ and ×) during the early period of solidification. As seen from Fig. 10, during the early period of the solidification, it is notable that the isothermal lines are inclined to the cold wall because of a natural convection caused by the temperature gradient at the upper part of the cell and the concentration gradient in the mushy region. As a natural convection zone becomes narrower and the thickness of the concentration stratification enlarges with the progress of the solidification, the convection is weakened, and then the isothermal lines gradually become parallel to the cold wall. Isothermal lines at $t = 120$ min for the cases of three kinds of beads are obtained as in Fig. 10(b) and Fig. 11. The heat conduction dominates the temperature field in the case where the effective thermal conductivity is high, therefore in the case of steel beads the experimental results shown by the solid lines and the calculated results shown by the dashed lines are nearly parallel to the cold wall as shown in Fig. 11(b). On the other hand, for the case of vinyl chloride beads that have the lowest thermal conductivity of the three kinds of beads, the effect of natural convection on the temperature field is the strongest, as shown in Figs. 10(b) and 11.

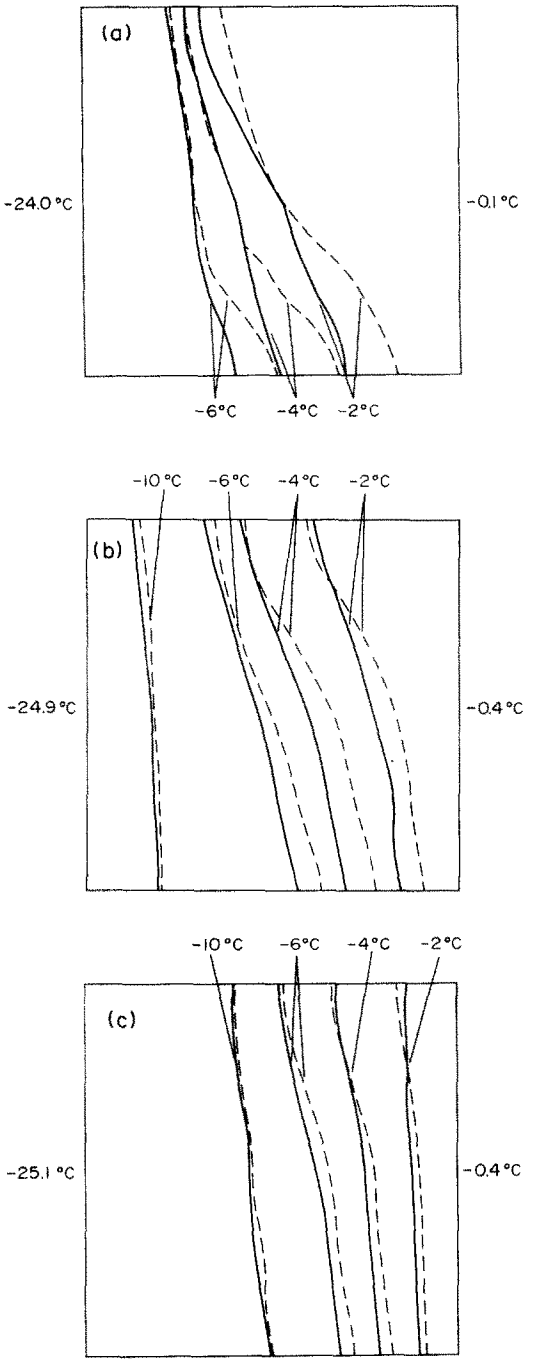

FIG. 10. Temperature distribution in the case of vinyl chloride beads. —— Experimental results. --- analytical results. $C_i = 10$ wt(%), $T_B = -30$°C, $D_b = 3.76$ mm. (a) $t = 60$ min. (b) $t = 120$ min. (c) $t = 240$ min.

Time-dependencies of the position of the freezing front obtained analytically are shown in Fig. 12. The solid, dashed and chain lines show the cases of vinyl chloride, glass and steel beads, respectively. As is evident from Fig. 12, the growth rate of the freezing front at the lower part of the cell is slower than that at the middle section of the cell. At the upper section of the

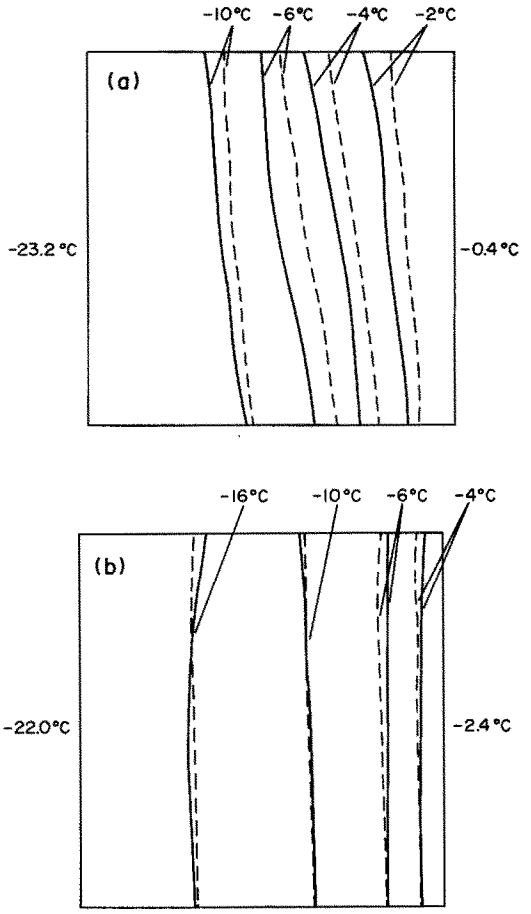

FIG. 11. Temperature distribution. —— Experimental results, --- analytical results. $C_i = 10$ wt(%), $T_B = -30°C$, $t = 120$ min. (a) Glass beads with $D_b = 2.56$ mm. (b) Steel beads with $D_b = 2.76$ mm.

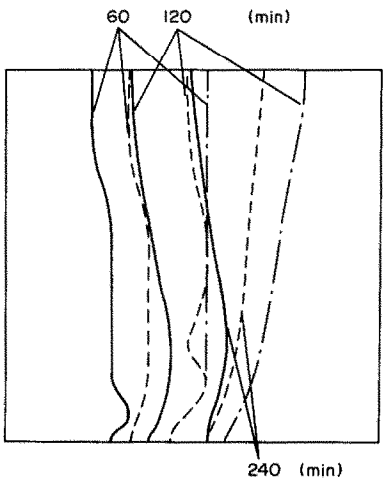

FIG. 12. Time-dependency of calculated freezing front. $C_i = 10$ wt(%), $T_B = -30°C$. —— Vinyl chloride beads with $D_b = 3.76$ mm. --- Glass beads with $D_b = 2.56$ mm. –·– Steel beads with $D_b = 2.76$ mm.

cell, high-temperature liquid heated by the hot wall is transported to the freezing front due to the natural convection, therefore, the growth rate of the freezing front is suppressed at the initial time of solidification. But as the natural convection is suppressed by concentration stratification, its growth rate at the upper part of the cell becomes larger than that at the middle section of the cell according to time. Therefore, geometry of the freezing front except for near the bottom of the cell becomes gradually parallel to the cold wall according to time. From comparison of solid lines with dashed lines, it is found that the growth rate of the freezing front increases as the thermal conductivity of the beads increases, but there is no qualitative difference for time-dependency of the freezing front geometry between the different kinds of beads.

The results of time-dependency of the concentration in the case of glass beads are shown in Fig. 13. These results are obtained by the analysis. From these figures, it is clarified that the thickness of the concentration stratification formed in the liquid region enlarges upwards as time increases. Similar analytical results in the cases of steel and vinyl chloride beads are shown in Figs. 14 and 15, respectively. From Figs. 13(b), 14 and 15, as the growing rate of the freezing front in the case of steel beads is faster than that in the other two cases, the amount of solute rejected from the solution in the mushy region and transported to the liquid region in the case of steel beads is larger than that in the other two cases. Therefore, the thickness of the high concentration layer (e.g. 11 wt(%)) in the case of steel beads is the largest among the three cases.

Next the constant volume fraction lines shown in Figs. 13–15 will be discussed. The constant volume fraction lines of $(\chi/\Phi) = 0.5$ and 0.7 just above the bottom wall are inclined to the cold wall, because the high concentration layer on the bottom of the cell suppresses the progress of solidification in the mushy region, although the temperature in the lower part of the cell is low. A few projection-wise changes are observed in the constant volume fraction lines, for example $(\chi/\Phi) = 0.5$ or 0.7 in Fig. 13(a). As shown in Fig. 2, when (χ/Φ) is larger than 0.7, the value of the permeability increases rapidly. Therefore, the permeability in the case where the value of (χ/Φ) is nearly equal to 0.7 sensitively influences the flow in the mushy region. The volume fraction of liquid phase is obtained from equations (7)–(9) and is dependent on the velocity, temperature and concentration, which are complexly connected with each other. Therefore, the constant volume fraction lines of $(\chi/\Phi) = 0.7$ and 0.5 change complexly as shown in Figs. 13(b), (c). As the high concentration layer in the mushy region enlarges upward with the progress of solidification, the projection-wise changes of the constant volume fraction lines appear in the higher part of the cell.

The calculated results of the stream function in the mushy region and the liquid region are shown in

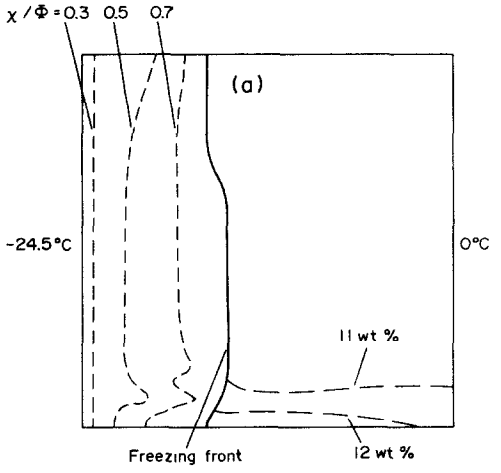

FIG. 13. Distributions of calculated concentration and volume fraction in the case of glass beads. $C_i = 10$ wt(%), $T_B = -30°C$, $D_b = 2.56$ mm. (a) $t = 60$ min. (b) $t = 120$ min. (c) $t = 240$ min.

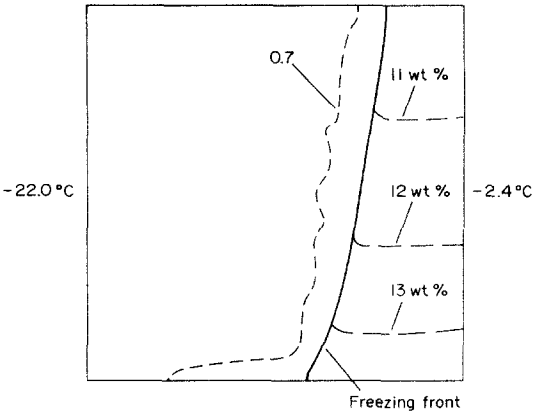

FIG. 14. Distributions of calculated concentration and volume fraction in the case of steel beads. $C_i = 10$ wt(%), $T_B = -30°C$, $D_b = 2.76$ mm, $t = 120$ min.

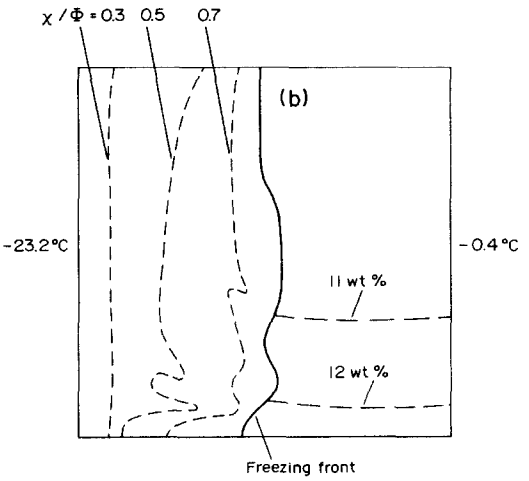

Fig. 16. From Fig. 16, it is clarified that a natural convection occurs in the whole liquid region at the initial period, but the natural convection zone moves upward and the natural convection is suppressed by the concentration stratification after some time. The natural convection in the mushy region occurs only near the freezing front.

For heat flux in the case of vinyl chloride beads, a good agreement between experimental results and analytical results was obtained, as shown in Fig. 17.

5. CONCLUSIONS

The solidification process from one vertical wall of the rectangular cell in which beads saturated with NaCl-solution were packed was investigated analytically and experimentally. In the experiment, the

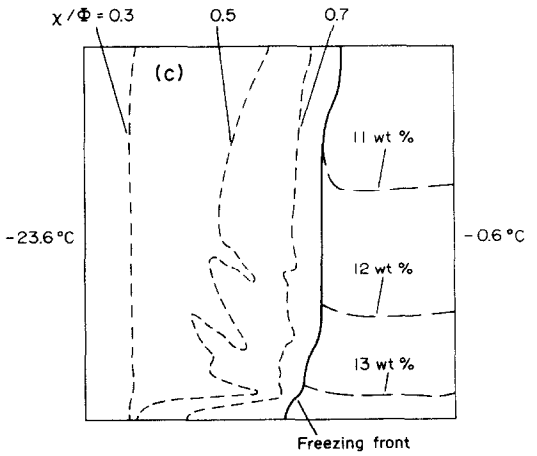

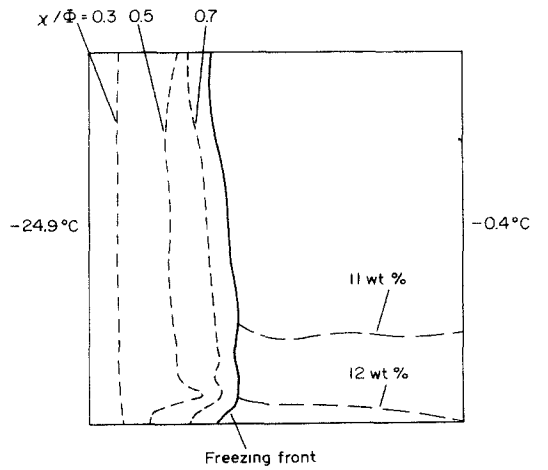

FIG. 15. Distributions of calculated concentration and volume fraction in the case of vinyl chloride beads. $C_i = 10$ wt(%), $T_B = -30°C$, $D_b = 3.76$ mm, $t = 120$ min.

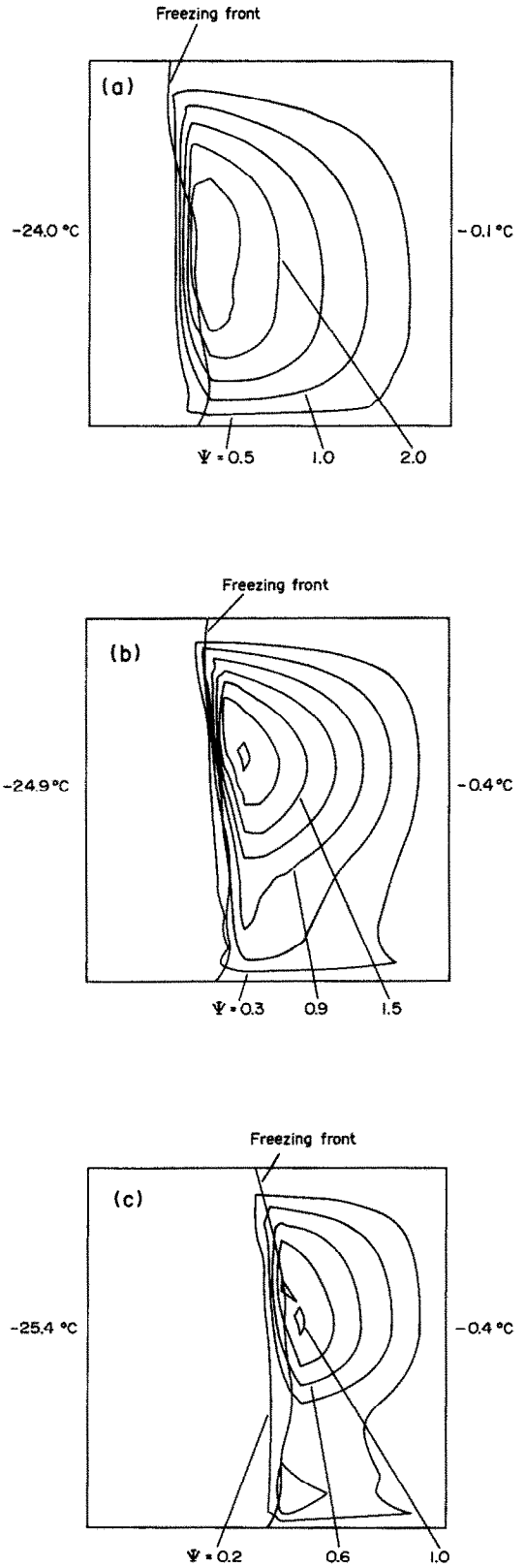

FIG. 16. Distribution of stream function in the case of vinyl chloride beads. $C_i = 10$ wt(%), $T_B = -30°C$, $D_b = 3.76$ m. (a) $t = 60$ min; interval of stream line = 0.5. (b) $t = 120$ min; interval of stream line = 0.3. (c) $t = 240$ min; interval of stream line = 0.2.

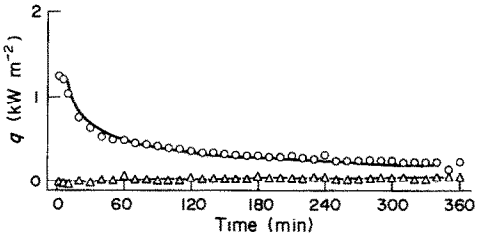

FIG. 17. Time-dependency of heat flux in the case of vinyl chloride beads. $C_i = 10$ wt(%), $T_B = -30°C$, $D_b = 3.76$ mm. ○ Experimental result at cold wall; —— analytical result at cold wall. △ Experimental result at hot wall; - - - analytical result at hot wall.

temperature and concentration distributions were measured for three kinds of beads with almost the same mean diameters.

Comparing the analytical results with the experimental results, the conclusions were obtained as follows.

(1) The present solidification process could be simulated approximately by the analysis, where permeability within the mushy region was expressed as $k/k_0 = (\chi/\Phi)^n$ ($n = 14$).

(2) It was found that the influence of the thermal conductivity of beads on the permeability in a state of solidification of porous medium saturated with NaCl-solution was very small for the size of the present experimental cell.

(3) The natural convection occurred in the whole liquid region at the initial period of solidification, but the natural convection zone moved upward and the natural convection was suppressed by the concentration stratification according to time. The natural convection in the mushy region occurred only near the freezing front.

(4) Several projection-wise changes were observed in the constant volume fraction lines of $(\chi/\Phi) = 0.5$ and 0.7.

Although the analysis approximately simulates the solidification process, the analytical results do not completely agree with the experimental results. It is considered that the difference is mainly caused by the assumption that the permeability in the mushy region is a function of only the volume fraction of the liquid phase in the mushy region. The authors consider that this permeability should be studied in more detail.

Acknowledgement—The authors wish to thank Mr Nonobe, a former student of Aoyamagakuin University, for his great co-operation in the experiment and Mr Howarth, a lecturer of Aoyamagakuin University, for his helpful advice.

REFERENCES

1. M. Sugawara, K. Kimoto and H. Jinushi, Freezing of a horizontal porous layer including water, *Trans. Japan Soc. Mech. Engrs* Series B **51**(464), 1285–1289 (1985).

2. S. Chellaiah and R. Viskanta, Freezing of saturated and superheated liquid in porous media, *Int. J. Heat Mass Transfer* **31,** 321–330 (1988).
3. M. Okada, Freezing around two cooled pipes in Darcy flow, *Heat Transfer—Jap. Res.* **9**(3), 54–69 (1980).
4. M. Okada, Approximate analysis of freezing around two cooled pipes in Darcy flow, *Heat Transfer—Jap. Res.* **9**(3), 70–87 (1980).
5. M. Okada, K. Kimura and I. Watanabe, Analysis of the freezing around a chilled pipe in Darcy flow, *Sixth International Heat Transfer Conference*, Toronto, Canada, August, Vol. 3, EN-6, pp. 31–36 (1978).
6. M. Epstein and D. H. Cho, Melting heat transfer in steady laminar flow over a flat plate, *ASME J. Heat Transfer* **98,** 531–533 (1976).
7. S. Chellaiah and R. Viskantata, Natural convection flow visualization in porous media, *Int. Commun. Heat Mass Transfer* **14,** 607 616 (1987).
8. M. Kazmierczak, D. Poulikakos and D. Sadowski, Melting of a vertical plate in porous medium controlled by forced convection of a dissimilar fluid, *Int. Commun. Heat Mass Transfer* **14,** 507–517 (1987).
9. M. Okada and T. Fukumoto, Melting around a horizontal pipe embedded in a frozen porous media, *Trans. Japan Soc. Mech. Engrs* Series B **48**(434), 2041–2047 (1982).
10. Y. Hayashi and T. Komori, Investigation of freezing of salt solution in cells, *ASME J. Heat Transfer* **101,** 459 464 (1979).
11. F. P. Incropera, A. H. H. Engel and W. D. Bennon, Numerical analysis of binary solid–liquid phase change with buoyancy and surface tension driven convection, *Numer. Heat Transfer* Part A **16,** 407–427 (1989).
12. C. Beckermann and R. Viskanta, An experimental study of binary mixtures with double-diffusive convection in the liquid, *Exp. Thermal Fluid Sci.* **2,** 17–26 (1989).
13. H. Rumpf and A. R. Gupte, Einflusse der porositat und korngroß enverteilung im widerstandsgesetz der porenstromung, *Chemie-Ing-Techn.* **43,** 367–375 (1971).
14. M. Okada, K. Matsumoto, Y. Yabushita and M. Fukuzaki, Measurement of permeability in a state of solidification of porous media saturated with solution, *Proc. 3rd Asian Thermophysical Prop. Conf.*, Beijing, China, October, pp. 490–497 (1992).